



## OPEN ACCESS

# The importance of repulsive potential barriers for the dispersion of graphene using surfactants

To cite this article: Ronan J Smith *et al* 2010 *New J. Phys.* **12** 125008

View the [article online](#) for updates and enhancements.

## You may also like

- [A new cleaning process combining non-ionic surfactant with diamond film electrochemical oxidation for polished silicon wafers](#)  
Gao Baohong, Zhu Yadong, Liu Yuling et al.
- [Immunochromatographic assay using gold nanoparticles for measuring salivary secretory IgA in dogs as a stress marker](#)  
Aki Takahashi, Shigeru Uchiyama, Yuya Kato et al.
- [Ion-Pair Conductivity Theory IV: SPAN Surfactants in Toluene and the Role of Viscosity](#)  
Sean Parlia, Ponisseril Somasundaran and Andrei Dukhin

## The importance of repulsive potential barriers for the dispersion of graphene using surfactants

Ronan J Smith, Mustafa Lotya and Jonathan N Coleman<sup>1</sup>

School of Physics and CRANN, Trinity College Dublin, Dublin 2, Ireland

E-mail: [colemaj@tcd.ie](mailto:colemaj@tcd.ie)

*New Journal of Physics* **12** (2010) 125008 (11pp)


Received 16 July 2010

Published 13 December 2010

Online at <http://www.njp.org/>

doi:10.1088/1367-2630/12/12/125008

**Abstract.** We have dispersed graphene in water, stabilized by a range of 12 ionic and non-ionic surfactants. In all cases, the degree of exfoliation, as characterized by flake length and thickness, was similar. The dispersed flakes were typically 750 nm long and, on average, four layers thick. However, the dispersed concentration varied from solvent to solvent. For the ionic surfactants, the concentration scaled with the square of the zeta potential of the surfactant-coated flakes. This suggests that the concentration is proportional to the magnitude of the electrostatic potential barrier, which stabilizes surfactant-coated flakes against aggregation. For the non-ionic surfactants, the dispersed graphene concentration scaled linearly with the magnitude of the steric potential barrier stabilizing the flakes. However, the data suggested that other contributions are also important.

 Online supplementary data available from [stacks.iop.org/NJP/12/125008/mmedia](http://stacks.iop.org/NJP/12/125008/mmedia)

### Contents

<b>1. Introduction</b>	<b>2</b>
<b>2. Experimental details</b>	<b>2</b>
<b>3. Results and discussion</b>	<b>3</b>
3.1. Characterization of surfactant-stabilized graphene . . . . .	3
3.2. Stabilization mechanism for ionic surfactants . . . . .	7
3.3. Stabilization mechanism for non-ionic surfactants . . . . .	10
<b>4. Conclusion</b>	<b>11</b>
<b>Acknowledgments</b>	<b>11</b>
<b>References</b>	<b>11</b>

<sup>1</sup> Author to whom any correspondence should be addressed.

## 1. Introduction

Over the last few years, it has become clear that graphene will be extremely useful both for fundamental studies and for a range of applications [1, 2]. While graphene can be grown by chemical vapour deposition [3], it is most commonly obtained by exfoliation from graphite crystals. Where individual flakes on substrates are required, micromechanical cleavage is the exfoliation method of choice as it gives reasonably large, high-quality flakes [4]. However, some applications of graphene require large quantities that could never be produced by micromechanical cleavage. Examples are the use of graphene as a filler in polymer-based composites or as thin films or coatings. It has recently been shown that graphene can be produced in large quantities by exfoliation of graphite in certain solvents [5]–[10] or surfactants [11]–[14]. Of these methods, surfactant dispersion is perhaps the most promising because the use of toxic solvents is avoided. While such methods give reasonably large quantities of good-quality graphene, there is still much scope for improvement. For example, it is difficult to prepare high-concentration dispersions and flake sizes larger than  $1\ \mu\text{m}^2$ . In addition, the dispersed graphene comes as both mono- and multi-layers. It would be of great interest to develop high-concentration dispersions dominated by large-area monolayers.

To improve the concentration and quality of surfactant-stabilized graphene dispersions, it is critical that one gains an understanding of the physics and chemistry of the stabilization process. Such an understanding will aid surfactant choice and process optimization, resulting in better dispersions. In this work, we have prepared dispersions of graphene in a range of surfactants. We have measured the dispersed concentration and characterized the exfoliation state. We find that the graphene concentration is controlled by the size of the potential barrier that stabilizes the surfactant-coated flakes against aggregation.

## 2. Experimental details

The surfactants used in this study were mostly ionic surfactants: sodiumdodecylsulfate (SDS), dodecylbenzenesulfonic acid (SDBS), lithium dodecyl sulfate (LDS), cetyltrimethyl ammoniumbromide (CTAB), tetradecyltrimethylammonium bromide (TTAB), sodium cholate (SC), sodium deoxycholate (DOC) and sodium taurodeoxycholate (TDOC). However, four non-ionic surfactants were also used: IGEPAL CO-890, Triton X-100, Tween 20 and Tween 80. All these surfactants are known to be efficient in dispersing carbon nanotubes [15]–[17]. Molecular structures of the surfactants are shown in figure 1. All surfactants were purchased from Aldrich and used as supplied. For each surfactant type, 500 mg of graphite powder, purchased from Sigma–Aldrich (product number 332461), was added to 100 ml of aqueous surfactant solution ( $0.1\ \text{mg ml}^{-1}$  surfactant concentration) to give an initial graphitic concentration of  $5\ \text{mg ml}^{-1}$ . This mixture was sonicated using a sonic tip (a Sonics VX-750 ultrasonic processor with a flat head tip) for 30 min at 75% of the maximum power (i.e. 75% of 750 W nominal maximum power). The dispersion was left to stand overnight. The top 20 ml was decanted into a 28.5 ml vial and centrifuged (Hettich Mikro 22R) for 90 min at 1500 rpm. The top 10 ml was then decanted into a 14 ml vial. UV–Vis–IR absorption spectroscopy (Varian Cary 6000i) and zeta potential measurements were then carried out immediately. The dispersions were then left to stand for 1 week undisturbed and the absorption spectrum was measured again. For each surfactant type, this procedure was performed three times. The reported values for the

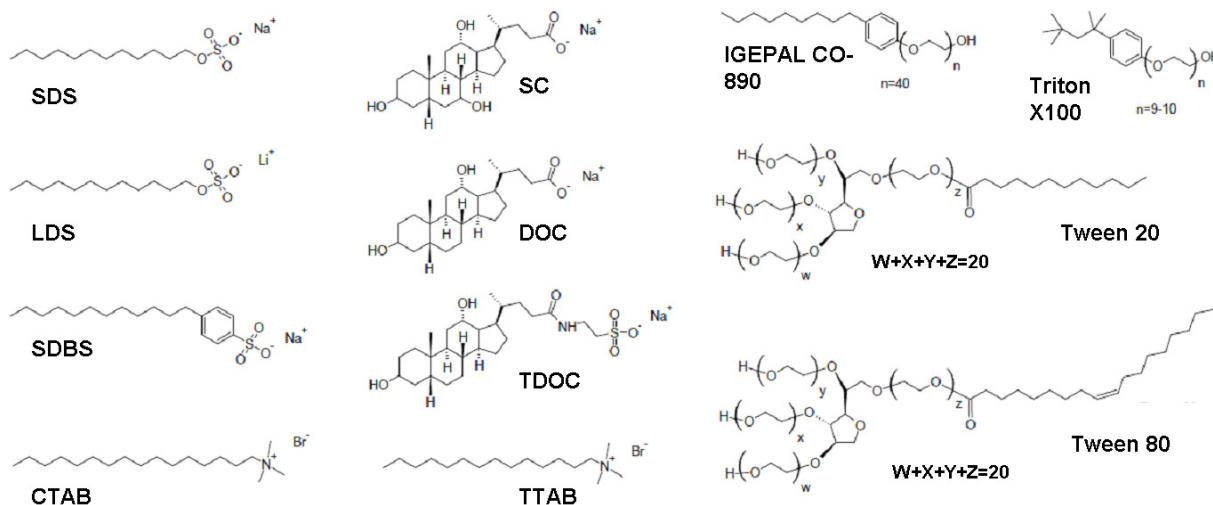


**Figure 1.** Structures of the surfactants used in this work.

concentration (calculated from the absorption spectra) and zeta potential are the averages over these three dispersions.

Graphene films were made by vacuum filtration of the dispersions immediately after centrifugation. A controlled volume of dispersion with known concentration was filtered through a nitrocellulose membrane (pore size 25 nm) and dried overnight in vacuum. This was then transferred to glass and the cellulose was dissolved in acetone. These films were then characterized by Raman spectroscopy. Ten spectra were collected from different parts of each film. The spectra were then normalized to the *G* peak and averaged. TEM grids (holey carbon) were prepared by drop casting immediately after centrifugation and dried overnight in vacuum.

Zeta potential measurements were carried out on a Malvern Zetasizer Nano system with irradiation from a 633 nm He–Ne laser. The samples were injected into folded capillary cells, and the electrophoretic mobility ( $\mu$ ) was measured using a combination of the electrophoresis and laser Doppler velocimetry techniques. The electrophoretic mobility relates the drift velocity of a colloid ( $v$ ) to the applied electric field ( $E$ ):  $v = \mu E$ . All measurements were carried out at 20 °C and at the natural pH of the surfactant solution, unless otherwise stated. The zeta potential can be calculated (in SI units) from the electrophoretic mobility using the Smoluchowski expression for plate-like particles [18]:  $\zeta = \eta\mu/\epsilon$ , where  $\eta$  is the solution viscosity and  $\epsilon$  is the solution permittivity  $\epsilon = \epsilon_r\epsilon_0$ . This expression applies to plates with uniform surface charge, which are large enough for the edge charge to be neglected and whose radii are much larger than the double layer thickness [19]. Since we estimated the double layer thickness (see the equation below) to be  $\sim 16$ – $24$  nm in our samples, we believe that these criteria hold here.

### 3. Results and discussion

#### 3.1. Characterization of surfactant-stabilized graphene

In this study, powdered graphite was dispersed in water using 12 different surfactants as stabilizers. In all cases, the surfactant concentration was very low,  $0.1 \text{ mg ml}^{-1}$  (this is below

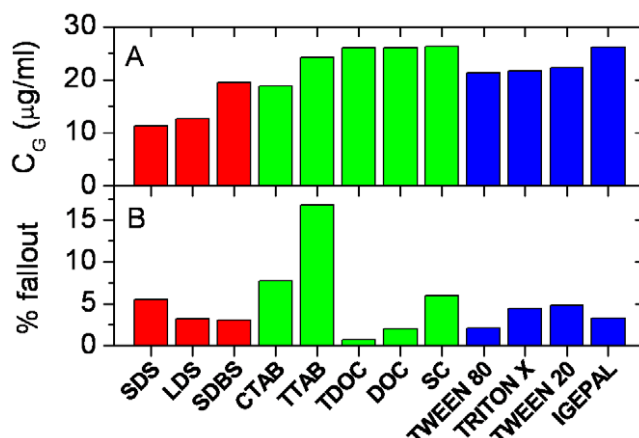


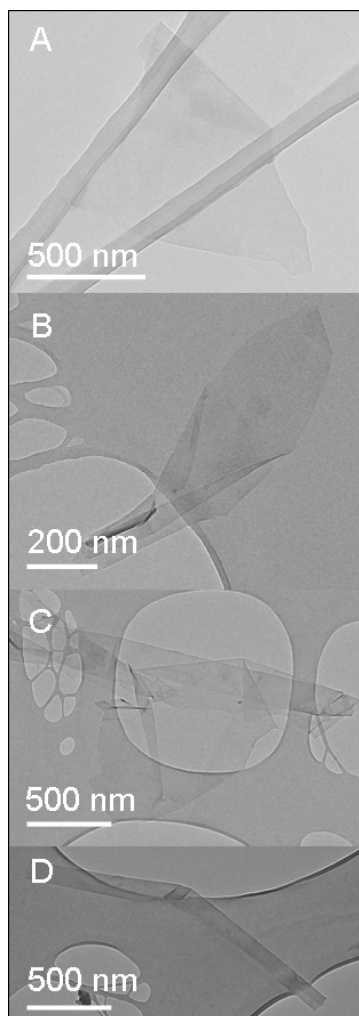
**Figure 2.** (A) Concentration of graphene remaining after centrifugation for dispersions stabilized with 12 different surfactants. (B) The amount of graphene that had sedimented after 7 days, expressed as a percentage of the original dispersed concentration. The data are colour coded to differentiate alkyl sulfates (SDS, SDBS and LDS, red), other ionic surfactants (green) and non-ionic surfactants (blue).

the critical micelle concentration (CMC) for all surfactants except Tween 80 and Tween 20; see supporting information available from [stacks.iop.org/NJP/12/125008/mmedia](http://stacks.iop.org/NJP/12/125008/mmedia)). The rationale behind this choice was twofold. Firstly, to aid direct comparison, it was necessary to prepare all dispersions identically. Previous work showed the optimum SC concentration to be  $0.1 \text{ mg ml}^{-1}$  [14]. However, the intrinsic advantage of using low surfactant concentrations is that there is less surfactant to remove if the dispersed graphene is to be used in applications such as transparent conductors [11]. The downside of this strategy is that as the dispersed concentration depends critically on the surfactant content, these dispersions are not optimized. Future work will involve comparing dispersed graphene for a range of surfactants, each at their optimum concentration.

The concentration of graphene remaining dispersed after centrifugation was calculated from the absorption spectra using an extinction coefficient of  $6600 \text{ ml}^{-1} \text{ g}^{-1}$  [14]. These concentrations are shown in figure 2(A) for all surfactants. The dispersed concentration varied from  $0.011 \text{ mg ml}^{-1}$  for SDS to  $0.026 \text{ mg ml}^{-1}$  for both SC and IGEPAL. We note that these concentrations are much lower than our previous values [14]. This is due to the fact that we used a sonic tip rather than a sonic bath in this work, to reduce the time required to prepare dispersions. It is interesting to note that the alkyl sulfate surfactants (red) are less effective than the other ionic surfactants (green) or non-ionic surfactants (blue).

We measured the stability of these dispersions by recording the absorption spectra (and so the concentration remaining dispersed) 7 days after sample preparation. We found that a small amount of graphene had sedimented over this period (figure 2(B)); with the exception of TTAB, in all cases  $<8\%$  of the graphene had fallen down over 7 days. In the case of TTAB,  $\sim 17\%$  fell out over the first week.

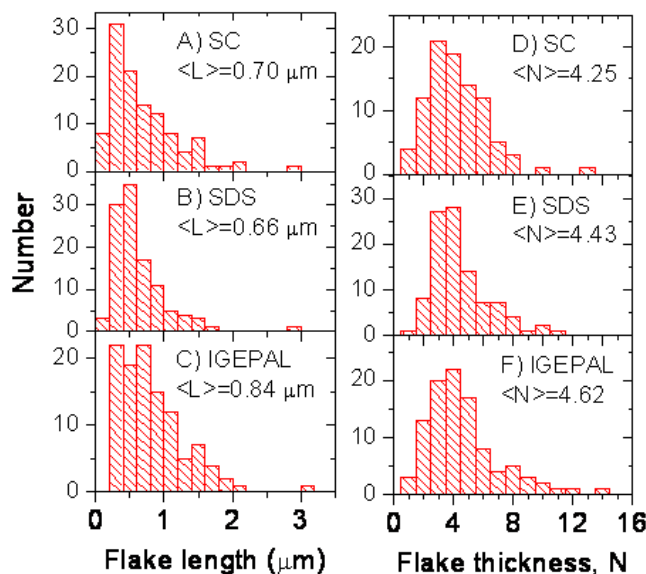
In order to determine the degree of graphene exfoliation, we performed TEM analysis on five of the dispersions (TDOC, SC, IGEPAL, SDS and TTAB). In all cases, large numbers of two-dimensional (2D) objects were observed. A selection of these is shown in figure 3. Of these,



**Figure 3.** TEM images of graphene flakes observed during this work.

A and B appear to be monolayers, whereas C is a multilayer. Objects resembling folded ribbons as shown in D are observed occasionally. Both broad flakes and ribbons were observed in all surfactants. All the objects observed tend to be of the type shown in figure 3 with no very large aggregates found.

The lateral size of the flakes is important for a number of applications. For example, for mechanical reinforcement in composites or thin conducting films, large flakes will be required. We measured the length of the long axis of a large number of flakes for the three surfactants discussed above: SDS, SC and IGEPAL. We chose these surfactants because they represent one from each family (alkyl sulfates, other ionics, and the non-ionics). In addition, they span the full range of dispersed graphene concentration from the lowest (SDS) to the highest (SC and IGEPAL). These data are presented in the form of histograms in figures 4(A)–(C). In each case, the flake length varies from  $\sim 100$  nm to  $\sim 3$   $\mu$ m. The mean length is close to  $0.75$   $\mu$ m in all cases. Such flake sizes are typical of graphene dispersed using solvents or surfactants [10, 13, 14]. It is also important that we estimate the degree of exfoliation of the flakes. We do this by measuring the flake thickness distribution for the same three surfactants by TEM



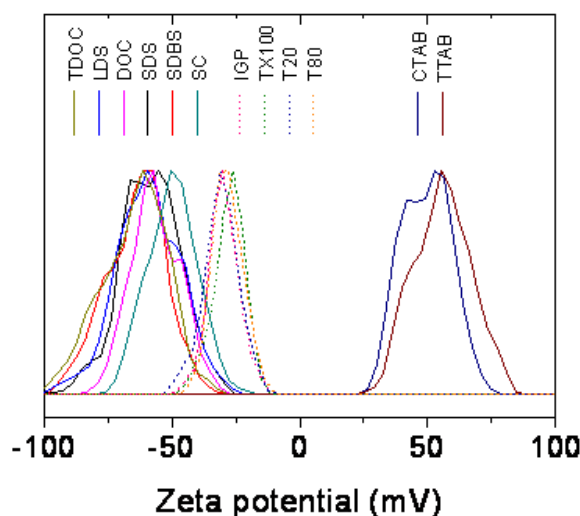
**Figure 4.** Statistical analysis of flake size. (A–C) Histograms showing flake length as measured by TWM for graphene dispersed in (A) SC, (B) SDS and (C) IGEPAL. (D–F) Histograms showing flake thickness, expressed as the number of graphene monolayers per flake, for graphene dispersed in (D) SC, (E) SDS and (F) IGEPAL.

image analysis, as described in detail in [10]. These data are shown in figure 4(D)–(F) as histograms of the number of monolayers per flake. In each case, flakes with thickness varying from 1 to 16 layers were observed with a mean flake thickness close to 4.5. It is interesting that each surfactant appears capable of exfoliating graphene to approximately the same degree.

We have also vacuum filtered some of the dispersions to form films (IGEPAL, TTAB, TDOC and SC). We have performed Raman spectroscopy on the films, measuring spectra at ten different positions before normalizing and averaging (SI). In each case, the spectra display well-defined D, G and 2D bands. The D/G ratio is between 0.25 and 0.6, typical of surfactant-stabilized flakes in this size range [14]. Such ratios suggest a defect population dominated by edge defects but with a small cohort of basal plane defects [14].

To summarize the results presented so far, graphene has been dispersed using 12 surfactants. The flake size and exfoliation state appear similar in each case. However, the dispersed concentration varies by a factor of 2–3 from surfactant to surfactant. It is critical that one gains an understanding of the factors that control the dispersed concentration. Any nano-scale object coated by surfactants is stabilized against re-aggregation by the presence of repulsive interactions between nearby surfactant-coated objects. All surfactants consist of a hydrophobic tail group and a hydrophilic head group. The nature of the repulsive interaction is controlled by the structure of the head group. While non-ionic surfactants have a polar head group, ionic surfactants have an ionic head group. Thus, for ionic surfactants, these repulsions are electrostatic in nature [20, 21], whereas for non-ionic surfactants, they can be due to a number of sources, such as steric interactions for molecules with bulky hydrophilic regions [21].





**Figure 5.** Zeta potential spectra for surfactant-stabilized graphene flakes for 12 different surfactants. The non-ionic surfactants are shown by dashed lines.

### 3.2. Stabilization mechanism for ionic surfactants

The source of the repulsions is most easily understood for ionic surfactants. In general, the surfactant tail group can adsorb by van der Waals (vdW) interactions onto non-polar objects, such as graphene flakes. In aqueous media, the head groups tend to disassociate, imparting an effective charge on the flake. The dispersed flakes will be stabilized by electrostatic repulsion between surfactant-coated flakes. In general, we do not consider the effective charge but rather the electric potential at the edge of the layer of bound ions: the zeta potential,  $\zeta$  [21]. The zeta potential can be measured in a straightforward manner for aqueous dispersions. We would expect the magnitude of the zeta potential to have a bearing on the graphene concentration that can be attained.

To test this, we measured the zeta potential distributions for graphene dispersed with each surfactant at the natural pH of the dispersion. These distributions are shown in figure 5 (see supporting information for the zeta potential distributions of the surfactants alone). The measured distributions are generally broad and asymmetric due to the range of flake sizes and possible contributions from free surfactant [17]. The distributions can clearly be divided into three sets: anionic, non-ionic and cationic. We estimated the zeta potential of the surfactant stabilized sheets to be the centre of the distribution. We found zeta potentials varying from  $-64$  mV for SDBS to  $+57$  mV for TTAB. The anionic surfactant-coated sheets had zeta potentials in the range  $-50$  to  $-64$  mV, whereas the cationic surfactants displayed zeta potentials of  $48$  and  $57$  mV. Interestingly, rather than being neutral, the graphene sheets coated by non-ionic surfactants displayed zeta potentials between  $-26$  and  $-31$  mV. This was previously observed for surfactant-stabilized nanotubes and may be due to adsorption of charged impurities [17]. We note that this means that even the graphene sheets coated with non-ionic surfactants may be partially stabilized by electrostatic interactions.

To test the relationship between the magnitude of zeta potential and the dispersed concentration, we plot  $C_G$  versus  $|\zeta|$  in figure 6(A). The data are clearly divided into three groups: the sulfides (SDS, SDBS and LDS), other ionic surfactants (TDOC, DOC, SC, TTAB



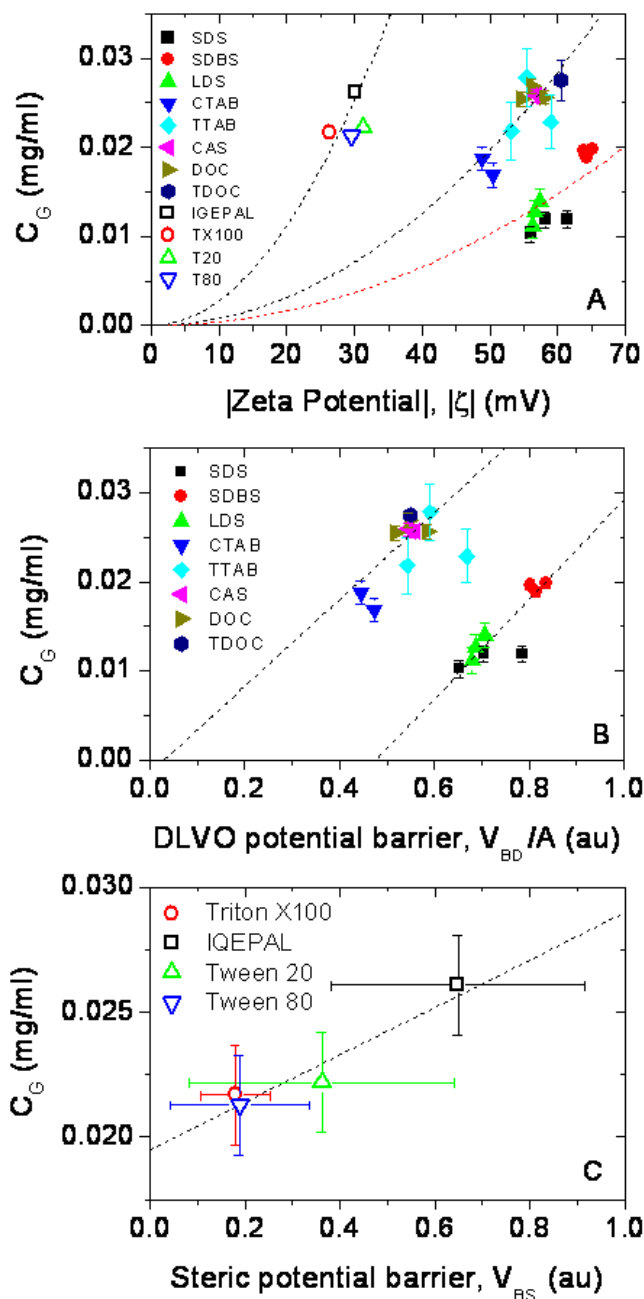


**Figure 6.** Dispersed graphene concentration (after centrifugation) plotted as a function of (A) the measured zeta potential of the dispersion and (B) the calculated potential barrier height due to Derjaguin–Landau–Verwey–Overbeek (DLVO) interactions between ionic surfactant-coated sheets. (C) The calculated potential barrier height due to steric interactions between non-ionic surfactant-coated sheets. The dashed lines in (A) represent  $C_G \propto \zeta^2$  behaviour.

and CTAB) and the non-ionic surfactants. Interestingly, for both groups of ionic surfactants,  $C_G$  clearly increases with increasing  $|\zeta|$ . Whereas such behaviour may occur for the non-ionic surfactant-stabilized systems, the data are too clustered to say definitively.

To understand this behaviour more clearly, we need to consider the stabilization mechanism in more detail. Within Derjaguin–Landau–Verwey–Overbeek (DLVO) theory, (ionic) surfactant-stabilized colloids are considered in terms of a layer of bound molecular ions (tail groups) and a diffuse cloud of counterions, the so-called double layer [21]. The repulsive DLVO potential energy for two charged surfaces is given by [21]:  $V_{\text{DLVO}} \approx 2A\epsilon_r\epsilon_0\kappa\zeta^2 e^{-\kappa D}$ , where  $\zeta$  is the zeta potential and  $\kappa^{-1}$  is the Debye screening length (a measure of the double layer thickness):  $\kappa^{-1} = (\epsilon_r\epsilon_0 kT/2e^2 n_0)^{1/2}$  ( $n_0$  is the number of surfactant molecules per unit volume of solution). We note that this expression strictly holds only for  $|\zeta| < 25$  mV. However, we use it here to illustrate the mechanism, realizing that any numbers generated will be approximate. We calculate the repulsive interaction energy for two charged 2D sheets by multiplying  $V_{\text{DLVO}}$  by 2 (to account for the fact that both sides of the sheets are charged). DLVO theory considers the balance of these repulsive interactions and attractive vdW interactions between adjacent colloids. The attractive vdW potential energy between two parallel 2D sheets can be approximated as the sum of pairwise inter-atom attraction energies. This can be calculated, in a manner [13] similar to the method pioneered by Hamaker [21], to be  $V_{\text{vdW}} = -A\pi\rho^2 C/2D^4$ , where  $A$  is the sheet area,  $\rho$  is the number of atoms per unit area in the sheets,  $D$  is the sheet separation and  $C$  is the constant relating the inter-atomic vdW energy to the inter-atomic separation:  $V = -C/r^6$ . We note that the expression does not account for screening or retardation effects. The overall potential energy of two parallel 2D sheets can thus be approximated as

$$V_T \approx 4A\epsilon_r\epsilon_0\kappa\zeta^2 e^{-\kappa D} - A\pi\rho^2 C/2D^4. \quad (1)$$

This function describes a potential that increases as  $D$  decreases, reaches a peak and then drops rapidly to a potential well. The well describes the case when the sheets are aggregated, while the peak represents a potential barrier against aggregation.

However, we previously showed that for graphene stabilized by SDBS [13], the potential barrier,  $V_{\text{BD}}$ , can be approximated by taking the value of the repulsive component as  $D$  approaches zero:  $V_{\text{BD}} \approx 4A\epsilon_r\epsilon_0\kappa\zeta^2$ . We suggest that the concentration of dispersed graphene may be strongly linked to the height of this potential barrier. In fact, we find that each of the three groups of data in figure 6(A) is consistent with  $C_G \propto \zeta^2$ , suggesting that  $C_G$  may scale linearly with  $V_{\text{BD}}$  (dashed lines). We can see this more clearly by plotting  $C_G$  as a function of  $\kappa\zeta^2$  (equivalent to plotting  $C_G$  versus  $V_{\text{BD}}/A$  in arbitrary units), as shown in figure 6(B). It is clear from this graph that the concentration of graphene stabilized by the non-alkyl sulfate ionic surfactants scales linearly with the barrier height with an intercept very close to zero. However, for the alkyl sulfates a different behaviour is observed. While the dependence of  $C_G$  on  $V_{\text{BD}}$  is linear, there is a significant intercept on the  $V_{\text{BD}}$  axis. This means that graphene can only be dispersed for electrostatic potential barriers above some minimum value. This suggests that the intersheet attractive potential is stronger for alkyl sulfate-coated sheets than for the other ionic surfactants. The origin of this additional attractive interaction is unknown at present.

That the dispersed concentration scales with barrier height immediately suggests that the dispersed concentration can be increased by taking steps to increase  $V_{\text{BD}}$ , by increasing either  $\zeta$  or  $\kappa$ . In practical terms, this would involve careful control of surfactant type and concentration. It is probably easiest to envisage increasing  $\zeta$  by surfactant control. As  $\zeta$  represents the electrostatic potential at the edge of the layer of bound ions, we can imagine increasing it by maximizing the surface charge in this layer. One can imagine choosing compact surfactants that pack tightly on the graphene surface to give high bound surfactant density. In addition, one can imagine increasing the charge per molecule by using multiply charged surfactants.

### 3.3. Stabilization mechanism for non-ionic surfactants

Having gained some insight into the dispersion mechanism of the ionic surfactants, we turn to the non-ionic surfactants. In each case, these surfactants have a hydrophobic tail and a long hydrophilic part. For such molecules, the stabilization mechanism tends to be based on steric effects [21]. The hydrophobic tail adsorbs on the graphene sheet, while the hydrophilic part extends into water. When two surfactant-coated sheets approach each other, the protruding hydrophilic groups begin to interact, resulting in an osmotic repulsion between the flakes. This results in a steric repulsive potential of the form:  $V_s \approx \alpha AkTL e^{-\pi D/L} s^{-3}$ , where  $\alpha$  is a constant,  $A$  is the flake area,  $L$  is the length of the protruding group and  $s$  is the average distance between adsorbed groups [21]. We note that this equation is appropriate for the case where the molecules are adsorbed at one end and closely packed on the surface. As usual, the total potential is the sum of this repulsive term and the vdW attractive term,

$$V_T \approx \frac{\alpha AkTL}{s^3} e^{-\pi D/L} - \frac{A\pi\rho^2 C}{2D^4}. \quad (2)$$

Assuming that, as with the electrostatic repulsive term above, one can approximate the potential barrier as the magnitude of the repulsive part as  $D$  approaches zero, we can write the barrier height as  $V_{BS} \approx \alpha AkTL/s^3$ . It is possible to estimate both  $L$  and  $s$  for the non-ionic polymers under study.

To estimate  $s$ , the average separation between adsorbed surfactant molecules, we assume them to be packed tightly onto the graphene surface. We estimate the combined area of the atoms in the hydrophobic part by counting the number of C atoms and multiplying this by an area per atom of  $(0.15 \text{ nm})^2 \times \pi/4$ . We consider the hydrophobic part as the region of the molecule to the left of the brackets in the structures of IGEPAL and Triton X-100 and to the right of the  $=O$  in the structures of Tween 20 and Tween 80 (figure 1). We take  $s$  as the square root of the hydrophobic area. To estimate  $L$ , we realize that closely packed, adsorbed linear molecules form brush-like structures. Here, the molecules tend to protrude away from the surface with a length that is proportional to the actual length of the protruding part of the molecule. We estimate this length from the number of bonds in the hydrophilic part of the molecule. While this is uncertain for the Tween surfactants, we estimate the maximum and minimum lengths, giving us a mean value. We also include relative errors of at least 10% in both  $L$  and  $s$ . This allows us to calculate  $L/s^3$  and so a value for  $V_{BS}$  in arbitrary units.

We plot  $C_G$  versus  $V_{BS}$  in figure 6(B). The data scale linearly, consistent with the hypothesis that the dispersed concentration does indeed scale with the potential barrier for steric stabilization [6]. However, note that the intercept on the concentration axis is  $\sim 0.02 \text{ mg ml}^{-1}$ . This suggests that even for very short, widely spaced protruding groups, a significant concentration of graphene would remain dispersed. This means that an additional stabilization mechanism must be present for these non-ionic surfactants. In fact the additional mechanism is most likely twofold. Each of the non-ionic groups has at least one acid group and many ether linkages. Such groups interact very strongly with water, making dispersion of surfactant-coated graphene flakes in water reasonably energetically favourable. In addition, we saw earlier that the non-ionic surfactant-coated graphene had a negative zeta potential, possibly due to adsorbed impurities. Such a zeta potential would result in an additional potential barrier, further stabilizing the flakes.

As in the case of ionic surfactants, we can speculate on non-ionic surfactant structures that would maximize the potential barrier. It is clear that a compact yet strongly bound tail group is

required to maximize the number of bound molecules per unit area of graphene sheet. The polar part of the surfactant must be very long and interact strongly with water via large numbers of hydrophilic groups ( $-\text{OH}$ ,  $-\text{COH}$ , etc).

#### 4. Conclusion

In conclusion, we have shown that graphene can be dispersed with the aid of a range of surfactants at low surfactant concentration. The dispersed flake size and degree of exfoliation (flake thickness) vary very little from surfactant to surfactant. However, the dispersed concentration varies from  $11 \mu\text{g ml}^{-1}$  for SDS to  $26 \mu\text{g ml}^{-1}$  for SC. We show that for ionic surfactants, the concentration is largely controlled by the zeta potential of the surfactant-coated graphene sheet. Specifically, the concentration scales linearly with the repulsive electrostatic potential barrier that stabilizes surfactant-coated sheets against aggregation. Similarly, for non-ionic surfactants, the concentration scales linearly with a repulsive potential barrier that has steric origins. However, in this case, other repulsive interactions are present. These may have both electrostatic and thermodynamic origins.

#### Acknowledgments

We thank SFI for support through a Research Frontiers Grant (09/RFP/MTR2286). ML thanks IRCSET for support.

#### References

- [1] Geim A K 2009 *Science* **324** 1530–4
- [2] Geim A K and Novoselov K S 2007 *Nat. Mater.* **6** 183–91
- [3] Reina A *et al* 2009 *Nano Lett.* **9** 30–5
- [4] Novoselov K S *et al* 2005 *Proc. Natl Acad. Sci. USA* **102** 10451–3
- [5] Blake P *et al* 2008 *Nano Lett.* **8** 1704–8
- [6] Bourlinos A B, Georgakilas V, Zboril R, Steriotis T A and Stubos A K 2009 *Small* **5** 1841–5
- [7] Hamilton C E, Lomeda J R, Sun Z Z, Tour J M and Barron A R 2009 *Nano Lett.* **9** 3460–2
- [8] Hernandez Y, Lotya M, Rickard D, Bergin S D and Coleman J N 2010 *Langmuir* **26** 3208–13
- [9] Hernandez Y *et al* 2008 *Nat. Nanotechnol.* **3** 563–8
- [10] Khan U, O'Neill A, Lotya M, De S and Coleman J N 2010 *Small* **6** 864–71
- [11] De S *et al* 2009 *Small* **6** 458–64
- [12] Green A A and Hersam M C 2009 *Nano. Lett.* **9** 4031–6
- [13] Lotya M *et al* 2009 *J. Am. Chem. Soc.* **131** 3611–20
- [14] Lotya M, King P J, Khan U, De S and Coleman J N 2010 *ACS Nano*. **4** 3155–62
- [15] Wenseleers W, Vlasov II, Goovaerts E, Obraztsova E D, Lobach A S and Bouwen A 2004 *Adv. Funct. Mater.* **14** 1105–12
- [16] Sun Z, Nicolosi V, Rickard D, Bergin S D, Aherne D and Coleman J N 2008 *J. Phys. Chem. C* **112** 10692–9
- [17] White B, Banerjee S, O'Brien S, Turro N J and Herman I P 2007 *J. Phys. Chem. C* **111** 13684–90
- [18] Ohshima H 2006 *Theory of Colloid and Interfacial Electric Phenomena* ed A Hubbard (Amsterdam: Elsevier)
- [19] Sherwood J D and Stone H A 1995 *Phys. Fluids* **7** 697–705
- [20] Hunter R J 1993 *Introduction to Modern Colloid Science* (Oxford: Oxford University Press)
- [21] Israelachvili J 1991 *Intermolecular and Surface Forces* (New York: Academic)